Visual Abstract

Influence of Pr_6O_{11} addition on structural and magnetic properties of mechanically alloyed $Fe_{65}Co_{35}$ nanoparticles

Nacira Djellal
L3M, Département de science et génie des matériaux, Ecole nationale supérieure des mines et métallurgie, Annaba 23000, Algérie
nacira.djellal@ensmm-annaba.dz

Djamel E. Mekki
LESIMS, Department of Physics, Faculty of Science, University of Badji Mokhtar, BP. 12, Annaba, 23000, Algeria
djameleddinemekki@gmail.com

Elena Navarro, Pilar Marin
Instituto de Magnetismo Aplicado (UCM-ADIF), 28230 Las Rozas, Madrid, Spain
Departamento de Física de Materiales, Universidad Complutense de Madrid (UCM), 28040 Madrid, Spain
enavarro@ucm.es, mpmarin@fis.ucm.es

ABSTRACT. This work focuses on the synthesize of nanostructured $(Fe_{65}Co_{35})_{100-x}$ $(Pr_6O_{11})_x$ (x = 0, 5) powders using high energy ball milling. The influence of Pr_6O_{11} on structural, morphological and magnetic properties of $Fe_{65}Co_{35}$ nanoparticles were carried out by X-ray diffraction (XRD), scanning electron microscopy (SEM) with a dispersive energy analyzer (EDS), vibratory sample magnetometer (VSM) and differential scanning calorimetry (DSC). Results show that the praseodymium oxide addition increased the decrement rate of the crystallite size with milling time of about 27 % and decreased the increment rate of the internal micro-strain of 50 %. Moreover, because of its high grain fragmentation tendency, Pr_6O_{11} increases the hardness and brittleness of Fe-Co powders. Moreover, it minimized the cold welding between Fe-Co ductile particles leading to a significant decrease in the average particle size (~1µm). The magnetic measurements conducted at room temperature show that the saturation magnetisation (M_s) and the coercivity (H_c) increased with milling time in both compositions. A low M_s and high H_c values were detected in $(Fe_{65}Co_{35})_{95}$ $(Pr_6O_{11})_5$ nanoparticles. The results demonstrated a soft ferromagnetic nature in all of the synthesized nanoparticles with M_s in the range 207 – 216 emu/g and H_c is found to be 113 Oe.

Citation: Djellal, N., Mekki, D. E., Navarro, E., Marin, P., Influence of Pr6O11 addition on structural and magnetic properties of mechanically alloyed Fe65Co35 nanoparticles, Frattura ed Integrità Strutturale, 60 (2022) 392-406.

Received: 14.01.2022
Accepted: 10.03.2022
Online first: 12.03.2022
Published: 01.04.2022

KEYWORDS. Fe-Co; Pr_6O_{11}; Nanoparticles; Mechanical alloying; Cold welding; Fracture.

INTRODUCTION

A wide literature shows that transition metal-based nanostructured magnetic alloys, such as Fe, Co or Ni, pure or doped, have become the subject of large-scale researches, due to their particular characteristics, such as high saturation magnetization, M_s, a relatively low coercive field, H_c, and a fairly substantial Curie temperature, T_c [1–3]. These significant properties are related to the intrinsic characteristics of their constitutive elementary chemical elements, known to be ferromagnetically characterized by 3d-itinerant magnetism [4–6]. Nanostructured Fe-Co alloys belong to the soft magnetic systems since the magnetocrystalline anisotropy of these systems is attributed to a random distribution of the constituent crystallites and this, when the average size of the latter is smaller than the magnetic exchange length [7]. For all these reasons, the Fe-Co nanosystem admits various applications such as hyperthermia magnetic treatment [8,9], high density data storage devices [10], MRI contrast [11], absorption of microwaves [12] or as magnetic charge vectors in new generation magnetorheological fluids [13]. However, the magnetic properties that they admit are strongly influenced by the relative elementary concentrations as well as synthesise methods [14]. Numerous studies have therefore been carried out to answer these questions, it was shown from the Slater-Pauling curve that alloy based on Fe and Co, having the greatest magnetization and therefore the highest saturation magnetization at the ratio of 65 % Fe and 35 % Co [15]. In addition, specific techniques and development approaches have been adopted to synthesize nanostructured Fe-Co. Some chemicals, including electrochemical deposition, thermal decomposition from organometallic precursors, co-precipitation or even co-reduction in polyol [16–20] and others physical, including laser ablation [21,22] or mechanical alloying (MA) process, one of the most widely used because of its energy, low costs and relatively easy use [23–27]. During MA process, the powder particles are subjected to severe mechanical deformations and are repeatedly deformed, heat-treated (cooling and heating), welded and fractured leading to their gradual refinement at the nanoscale [28]. Therefore, uncommon properties could appear. Nevertheless, it is important to note at this level that Fe-Co binary nanoalloys obtained by most of these techniques admit certain disadvantages which must be avoided, such as, the fact that they have magnetisation values strongly lower than their massive state [29], involving the use of subsequent heat treatments susceptible to relax the existing internal stresses and improve the crystallinity of the nanomaterial [30]. It is therefore natural that research has been oriented, among other things, in the direction of the doping process of Fe-Co nanosystem by various elements, to obtain enhanced properties. Thus, many works have concerned the doping of Fe-Co by transition metals (Cr [31,32], Sn [33], Ni [34], Al [35], Cu [36,37], V [21]), rare earths (Dy [38]), metalloids (Si [39,40]) or non-metals (C [41], O [42]). Generally, the saturation magnetization of these alloys is greater higher is the amount of the ferromagnetic elements. Another promising challenge that could be performed is the combination of complementary features of Fe-Co 3d-itinerant magnetism with rare-earth 4f- localized one. Moreover, the 4f rare metals exhibit a strong magnetic susceptibility and generally magnetocrystalline anisotropy due to the interactions between their orbital moment and the crystalline field, the fact of alloying them with a 3d metal induces their polarization and therefore, consolidate the magnetization of the alloy. For described reasons, the study of these compounds has a fundamental interest in magnetic coupling and the development of interface walls; also they have potential applications as permanent magnets, magnetic sensors and magnetic recording media [24]. Unfortunately, studies on rare earth-transition metal alloys are limited by the cost of rare elements and their low oxidation stability [43], hence the almost absence of works on this subject.

It is in this context that this research work takes place; it aims specifically to study the effect of Pr_6O_{11}, the most stable form of the praseodymium, on the structural, microstructural, morphological and magnetic properties of $Fe_{65}Co_{35}$ mechanically alloyed nanoparticles. To the best of our knowledge, no study has been reported in the literature.

MATERIALS AND METHODS

Initial Fe (Alfa Aesar, 99 %, d < 10 μm), Co (Alfa Aesar, 99.8 %, 1.6 μm) and Pr_6O_{11} (99.9 %) powders were used to prepare the corresponding compositions $(Fe_{65}Co_{35})_{1-x}(Pr_6O_{11})_x$ (x = 0 and 5 %) with high energy ball milling. The initial powders were mechanically alloyed, under air in the appropriate amounts, using a vibratory ball mill Retsch

MM 400 assisted with two cylindrical vials (25 ml, WC) and balls (10 mm, WC). The frequency of the milling was kept at 20 Hz for 1, 2, 3, 4 and 5 hours. The ball to powder ratio was maintained at 25:1, around 50 % of the vial volume was empty to assure suitable space for the process of milling. In order to prevent the excessive heating of the powders, the mechanical alloying was stopped 15 min after every 15 min of milling. The analyses of the structural properties were performed using the X-ray diffraction method in an X'Pert MPD diffractometer. The X-ray radiations were obtained using an anticathode of Copper with $\lambda_{K\alpha1}$ = 0.15406 nm. The analysis range of 2θ values position was 5-100° with scanning step of 0.02° and an exposure time one second by step. The refined crystallite size, lattice parameter and microstrain were obtained using maud software.

The morphology, chemical composition and distribution of the alloyed powders were followed with a JEOL-6100 Scanning Electron Microscope equipped with Energy Dispersive Spectrometry (EDS). The average particle size was estimated from scanning electron micrographs using software Image J. The determination of magnetic properties, at room temperature, of the powders was obtained using Quantum Design Physical Property Measurement System option Vibrating Sample Magnetometer. Structural phase transformations and magnetic ordered temperature were determined by differential scanning calorimetry method using DSC 404 Netzsch equipment. The measurements, in the temperature range from 25 °C to 1200 °C, were under protective nitrogen gas and with a heating rate of 30 °C/min.

RESULTS AND DISCUSSION

The present section is devoted to the presentation of results obtained on this innovative quaternary nano-material, never studied before. The investigations are related to structural and microstructural properties by XRD and DSC, morphological observations by SEM and magnetically study by VSM. All these results will be the subject of combined analyses in order to try to propose a coherent and self-consistent appreciation of its properties.

Structural properties

Fig. 1 shows the XRD spectrum of unmilled $(Fe_{65}Co_{35})_{95}$ $(Pr_6O_{11})_5$ mixture powders.

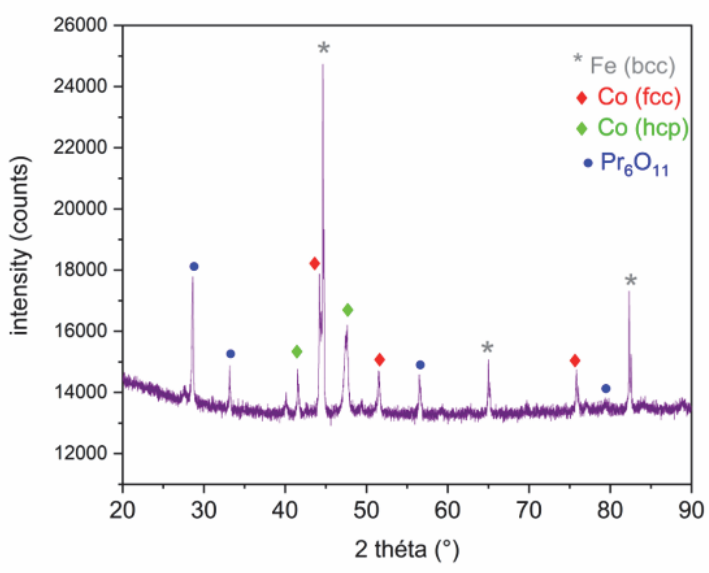

Figure 1: X-ray diffraction pattern of $(Fe_{65}Co_{35})_{95}(Pr_6O_{11})_5$ mixture

The spectrum of unmilled samples i.e., at t = 0 h, confirms the presence of the characteristic peaks of body centred cubic (BCC, COD 04-004-2474) iron, hexagonal close-packed (HCP, COD 04-006-6433) cobalt, face centred cubic (FCC, COD 04-015-0419) cobalt and fluorite cubic praseodymium oxide (COD 00-041-1219). The obtained phases match well with those given by the Joint Committee on Powder Diffraction (JCPDS). No additional characteristic peaks of any impurity phase were detected.

Fig. 2 characterizes the diffraction patterns of $Fe_{65}Co_{35}$ (Fig. 2.a) and $(Fe_{65}Co_{35})_{95}(Pr_6O_{11})_5$ (Fig. 2.b) powders at different milling times (t = 1, 2, 3, 4 and 5 h).

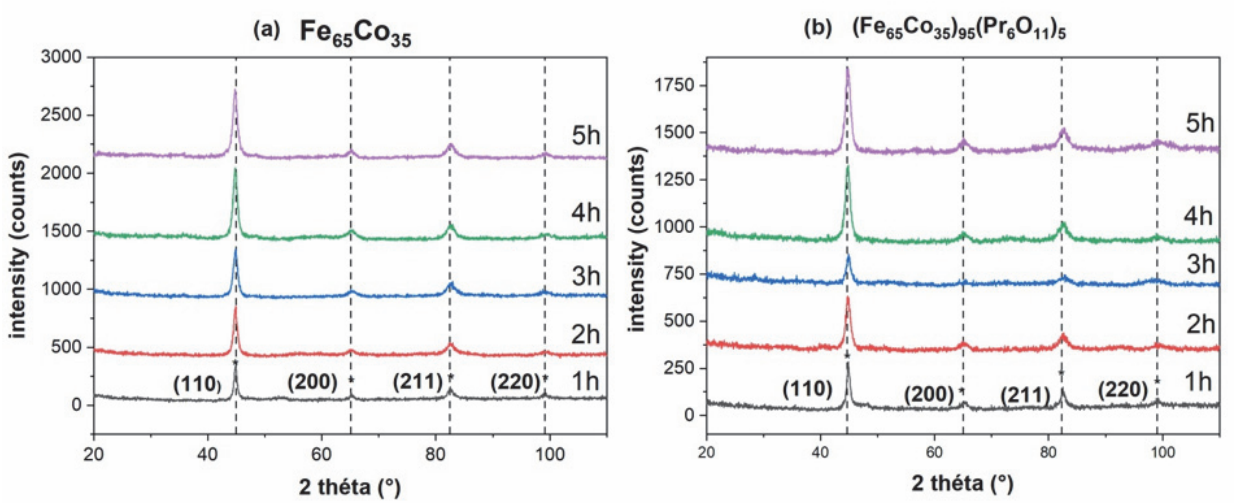

Figure 2: X-ray diffraction patterns of (a) $Fe_{65}Co_{35}$ and (b) $(Fe_{65}Co_{35})_{95}(Pr_6O_{11})_5$ mechanically alloyed powders at various duration (1, 2, 3, 4 and 5 h)

The figures display the XRD patterns of the powders for both compositions at different stages of mechanical alloying. As shown, both allotropic structures of Co (hcp and fcc) have disappeared after only one hour of milling, probably due to the high used vibration speed value (1200 rpm). Numerous results of literature show that, for lower values of rotational speed, of the order of 200 rpm, the final products are obtained in a more gradual manner, a process during which it can be appreciated the progressive transformation of fcc-Co to hcp-Co, followed by the disappearance of the latter, explained by the fact that Co atoms were totally incorporated into Fe BCC-structure [40,44,45]. For Pr_6O_{11}, the same evolution seems to occur; the characteristic peaks of Pr_6O_{11} have also disappeared after one hour of milling. The XRD spectrums at the different duration of milling identify only the Fe BCC phase and did not detect any additional peak of another phase (even working under air), which confirms the total dissolution of Co and Pr_6O_{11} into Fe structure and forming $(Fe_{65}Co_{35})_{100-x}(Pr_6O_{11})_x$ with (x = 0 and 5) alloys. It is relevant to note at this level, concerning the Fe-Co total solid solution, obtained under non-equilibrium conditions after one hour of milling, this result suggests that the Hume-Rothery rules, which are themselves qualitatively valid for metallic solutions determined at thermodynamic equilibrium, could also be applied for this type of material. The difference between Fe and Co atomic radii is less than 15 %, they also have the same valence (+2) which is necessary to reach a maximum solubility between atoms. Moreover, the electro-negativity values of Fe and Co are very close, 1.83 and 1.88 respectively, which leads to a high solubility between them [46,47]. On the other hand, there is no evidence for the quaternary system. With consecutive milling, a broadening of the peaks was observed. This enlargement is due to both increasing strain and decreasing crystallite size, which is typical behaviour of metallic alloys synthesized by mechanical alloying [40,48,49].

Fig. 3 presents the decrement of average crystallite size with milling time. On the other hand, Fig. 4 shows the evolution of micro-strains inside particles during mechanical alloying.

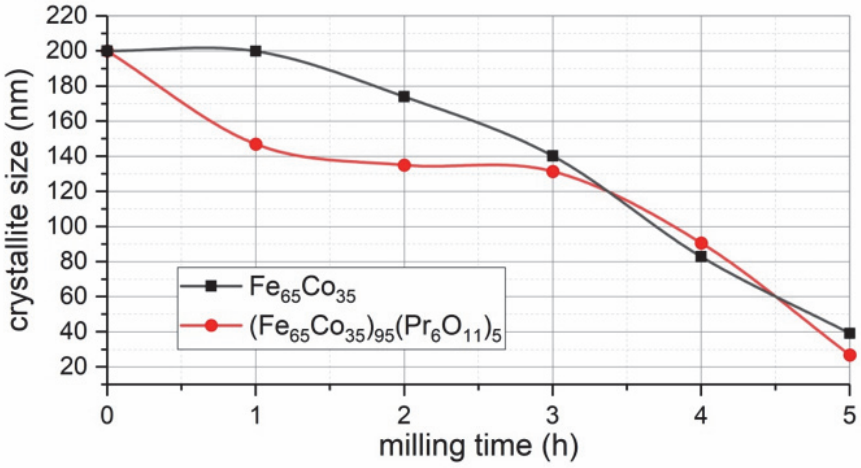

Figure 3: Refined crystallite size vs milling time

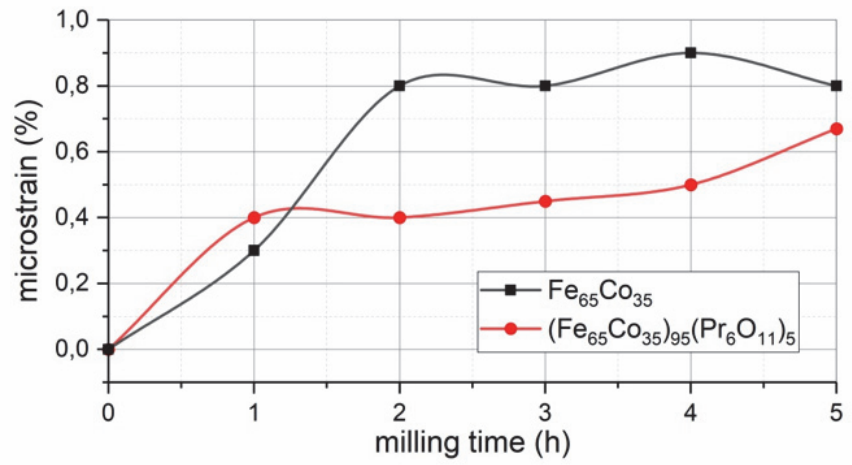

Figure 4: Refined microstrain vs milling time

The minimum value of crystallite size is about 20 nm reached after 5 h of milling in $(Fe_{65}Co_{35})_{95}(Pr_6O_{11})_5$ composition. For the microstrain, a similar tendency in both compositions is observed, it increases with milling time. However, the increment rate is higher at the early stage of milling. The maximum registered percentage of strain is about 1 % in $Fe_{65}Co_{35}$ powders milled for 3 h. In the mechanical alloying process, crystallites achieve a minimum size after a contest between dislocations generated from the consecutive deformation and dynamic recrystallization due to the relative increment of powders temperature during milling [15]. Fesht and Cantor [50,51] have proposed mechanisms describing the decreasing crystallite size process during mechanical alloying. In fact, during the beginning of the MA process, due to severe plastic deformation, a large number of defects (mainly dislocations) appear leading to the existence of local micro-deformations, whose intensity increases up to a certain onset where they stabilize by reorganizing themselves into random sub-joints of low disorientation. Last, at a certain moment and for different reasons (existence of precipitates...), the movement of dislocations is blocked, inducing the obtaining of constant average crystallite sizes. It can be observed that the addition of Pr_6O_{11} increases the strength and hardness of $Fe_{65}Co_{35}$. This is attributed to the hard nature of oxides leading to have high grain fragmentation tendency [52,53].

In both compositions, the refined lattice parameter decreased from 2.8660 nm (characteristic of bcc-Fe lattice), for unmilled powders, to 2.860 and 2.862 nm for $Fe_{65}Co_{35}$ and $(Fe_{65}Co_{35})_{95}(Pr_6O_{11})_5$ milled for 5 h respectively. This decrement refers to the following reasons: formation of triple defect disorders [7,45] and the substitution of Fe atoms by Co one with smaller diameter [7,52,54]. In $(Fe_{65}Co_{35})_{95}(Pr_6O_{11})_5$ composition, the decrement of lattice parameter suggests that the Pr_6O_{11}do not dissolve into the $Fe_{65}Co_{35}$ crystal lattice but dispersed in the Fe–Co matrix, probably at the grain boundaries.

Morphological observations

Fig. 5 presents the starting elemental powders and $(Fe_{65}Co_{35})_{95}(Pr_6O_{11})_5$ mixture morphologies. The micrographs show that the initial powders have a spherical and irregular shape of particles with few micrometres in size.

Fig. 6 (a-c) shows the evolving morphology of $Fe_{65}Co_{35}$ milled for 1, 3 and 5 h respectively, Fig. 6 (d-f) shows the $(Fe_{65}Co_{35})_{95}(Pr_6O_{11})_5$ powders milled for 1, 3 and 5 h respectively. The micrographs indicate that particles get small size and regular shape with milling time in both $Fe_{65}Co_{35}$ (Fig. 6.a-c) and $(Fe_{65}Co_{35})_{95}(Pr_6O_{11})_5$ (Fig. 6.d-f) powders. Fig. 6 (g-i) illustrates the quantitative average particle size of both compounds after 1, 3 and 5 h respectively.

The mechanical alloying process of ductile -fragile powders has been well explained conceptually by many authors [23,51,55,56]. In the case of (Fe, Co)-Pr_6O_{11} powders, the ductile particles (Fe, Co) undergo deformation while the fragile particles (Pr_6O_{11}) undergo fragmentation. Then, when the ductile particles start to cold welded, the fragile ones are placed between two or more ductile particles at the time of ball collision. As a result, the fragmented reinforcement particles are positioned on the interfacial boundaries of the welded Fe-Co particles, and the result is the formation of a real composite particle. These deformations, welding and solid dispersion phenomena harden the material and increase the fracture process, which also contributes to the formation of an equiaxed morphology. At this stage, the welding and fracture mechanisms reach an equilibrium favouring the formation of composite particles with a refined microstructure.

It is visibly seen the drastic decrease of particles size with milling time in both compositions (Fig. 6.g-i). After 1 h of milling, it clearly appeared that $Fe_{65}Co_{35}$ and $(Fe_{65}Co_{35})_{95}(Pr_6O_{11})_5$ nanoparticles fairly greatly agglomerate (Fig. 7.a and 7.d respectively), hence generating wide particle size distribution, whose average is estimated to 23 microns for $Fe_{65}Co_{35}$ and

12 microns for the quaternary system, (Fig. 6.g). This particle coalescence is explained in the literature by the presence of strong magnetic interactions in Fe-Co based alloys and also by the high surface energy in the grain boundaries of mechanically alloyed crystallites. In this stage of mechanical alloying, the powders are effectively subjected to continuous deformations leading to the cold welding, flattening and fragmentation of particles [46]. The micrographs at 3 h of milling show more regular shape of particles (Fig. 6.b for $Fe_{65}Co_{35}$ and Fig. 6.e for $(Fe_{65}Co_{35})_{95}(Pr_6O_{11})_5$) and drastic decrement in the average particles size (Fig. 6.h) in both compositions, besides, $(Fe_{65}Co_{35})_{95}$ $(Pr_6O_{11})_5$ powders are finer. This is can be explained by the fact that praseodymium oxide increases the hardness and brittleness of Fe-Co powders known to have a strong tendency to agglomerate [57]. The addition of Pr_6O_{11} leads to an increase in the grain fragmentation tendency of Fe-Co powders. The repeated plastic deformation, fracturing, cold welding and fragmentation of powder particles at this stage of milling severely introduced defects and structural disorders which may deteriorate the structural integrity of the nanoparticles [58,59]. Zhang et al. [60] and He et al. [61] found that the intense collisions involved in the high energy ball milling process severely damage the side walls of particles causing a decline in structural integrity of nanostructured powders. Therefore, an optimization of the milling time and speed are crucial to preserve the structural integrity. With further milling (up 5 h), the particles get a more uniform shape (Fig. 6.c, 6.f) and narrower particle size distribution (Fig. 6.i). At this stage, a balance between the fracture and cold welding is reached [54].
Fig. 7 presents the EDS elemental analysis in both compositions mechanically alloyed for 5 h.

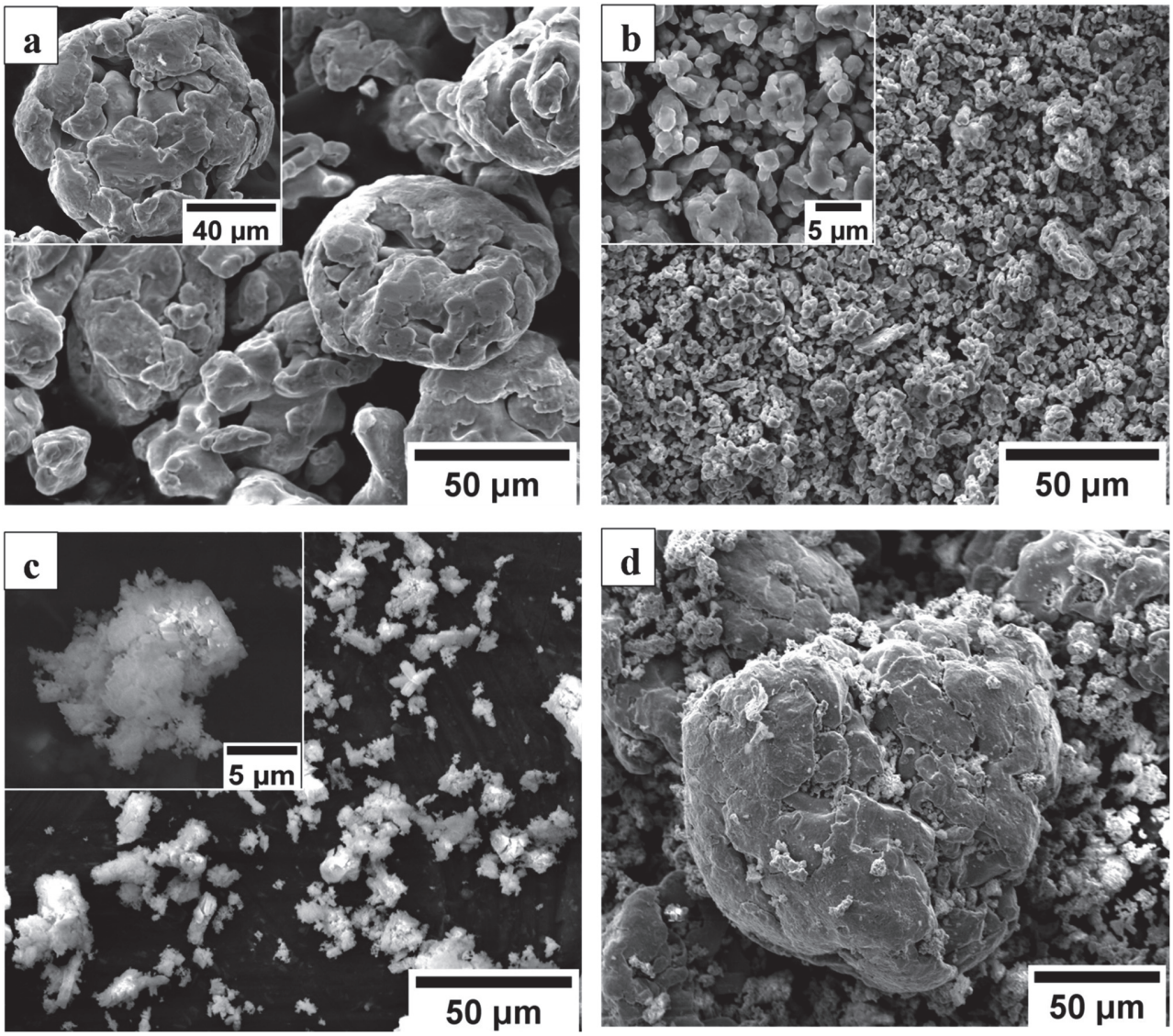

Figure 5: Scanning electron micrographs of as received powders (a) pure Fe; (b) pure Co; (c) pure Pr_6O_{11} and (d) $(Fe_{65}Co_{35})_{95}(Pr_6O_{11})_5$ mixture.

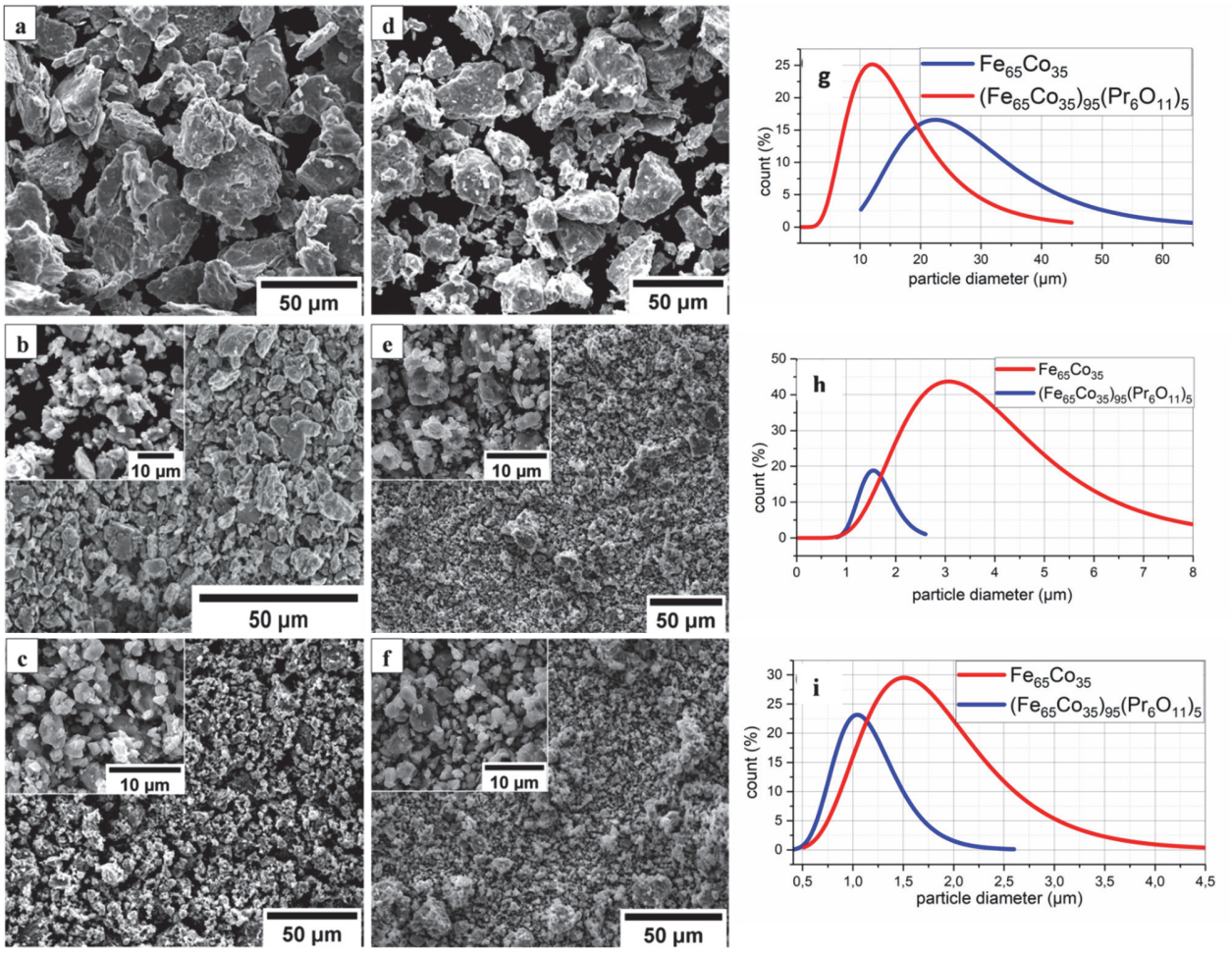

Figure 6: Scanning electron micrographs of $Fe_{65}Co_{35}$ mechanically alloyed for (a) 1 h; (b) 3 h; (c) 5 h and $(Fe_{65}Co_{35})_{95}(Pr_6O_{11})_5$ mechanically alloyed for (d) 1 h; (e) 3 h and (f) 5 h and the average particle size distribution of $Fe_{65}Co_{35}$ and $(Fe_{65}Co_{35})_{95}(Pr_6O_{11})_5$ mechanically alloyed for (g) 1 h; (h) 3 h and (i) 5 h.

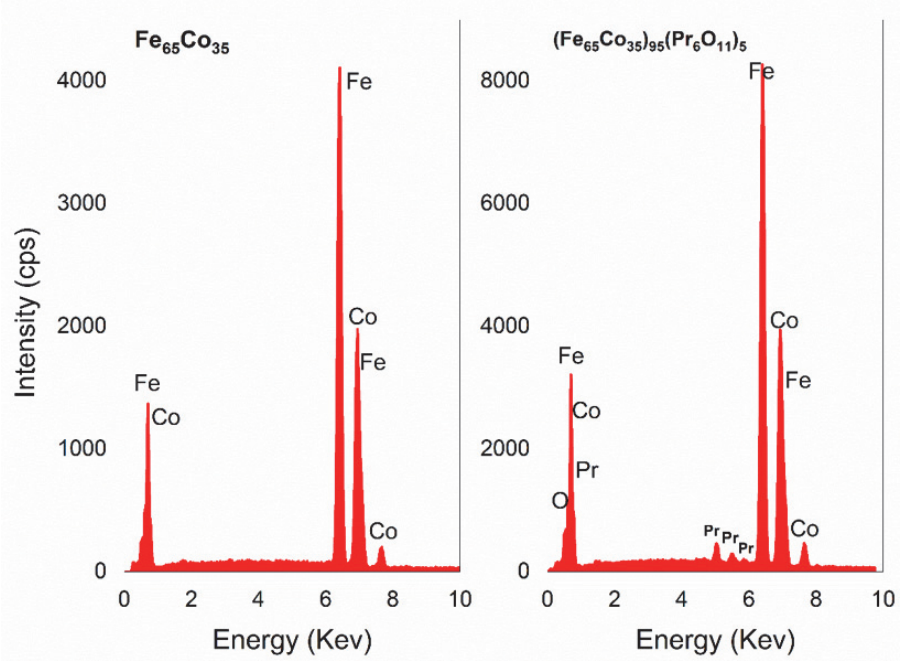

Figure 7: Energy dispersive spectrometry analysis of $Fe_{65}Co_{35}$ and $(Fe_{65}Co_{35})_{95}(Pr_6O_{11})_5$ mechanically alloyed for 5 h.

The analysis shows the presence of peaks belonging to Fe, Co in $Fe_{65}Co_{35}$ sample and Fe, Co, Pr and O in $(Fe_{65}Co_{35})_{95}(Pr_6O_{11})_5$ sample. In both alloys, no indication of impure elements was detected. Therefore, the contamination from vial or ball with other elements such as W is negligible.
Fig. 8 shows the elemental distributions in both alloys, that is, Fe and Co in $Fe_{65}Co_{35}$ (Fig. 8-a) and Fe, Co, Pr and O in $(Fe_{65}Co_{35})_{95}(Pr_6O_{11})_5$ one (Fig. 8-b).

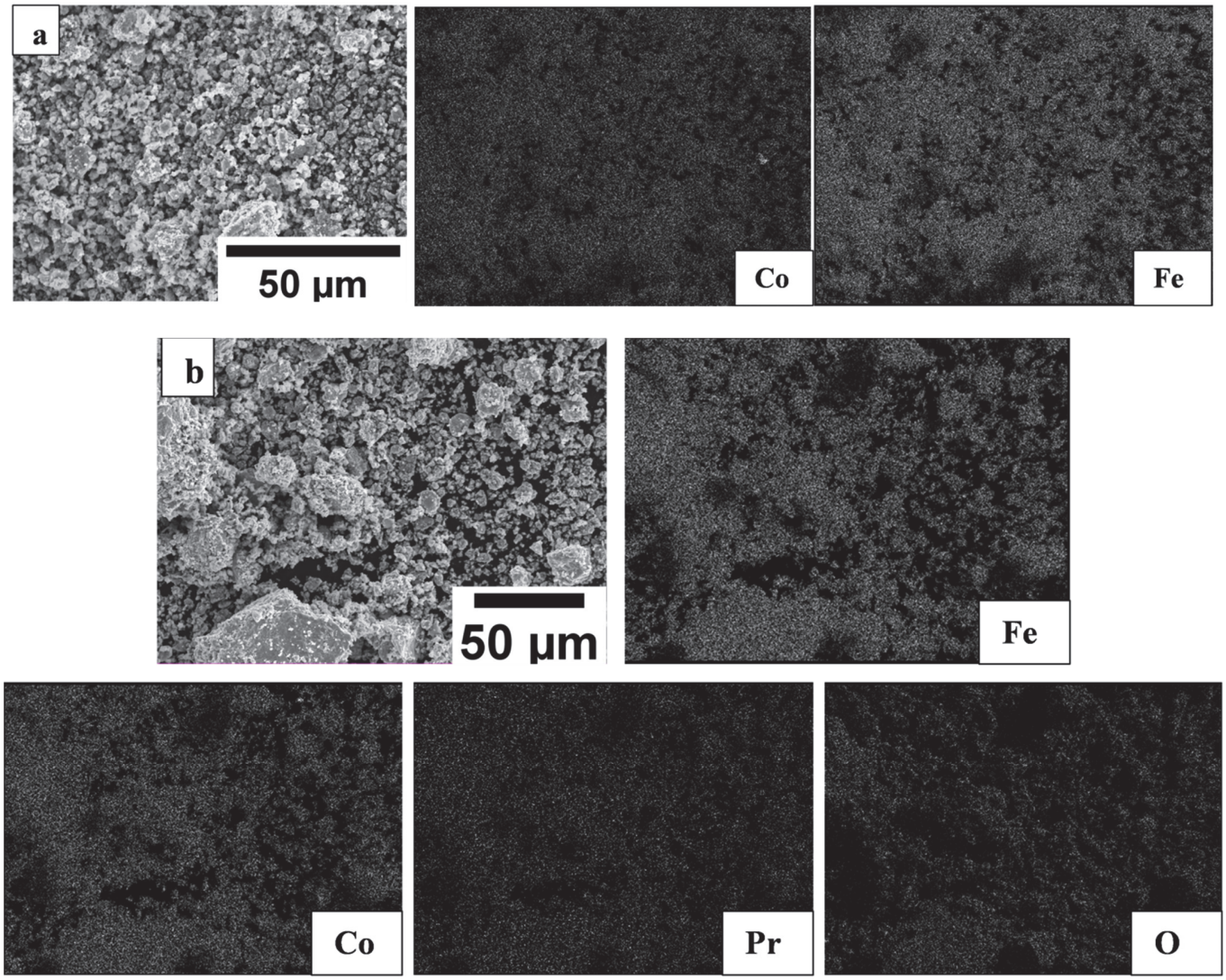

Figure 8: Scanning electron images with elemental distributions in (a) $Fe_{65}Co_{35}$ and (b) $(Fe_{65}Co_{35})_{95}(Pr_6O_{11})_5$ mechanically alloyed for 5 h.

All constituent elements seem uniformly and homogenously distributed inside particles after 5 h of milling. This indicates that the elements are completely alloyed and that solid solutions are formed. These findings are consistent with the previously obtained XRD results in this study.

MAGNETIC INVESTIGATIONS

It is widely admitted that the magnetic behaviour of ferromagnetic materials is strongly affected by crystallite size, chemical composition and internal defects. For this purpose, the study of the simultaneous effects of these parameters on $Fe_{65}Co_{35}$ and $(Fe_{65}Co_{35})_{95}(Pr_6O_{11})_5$ magnetic properties has been undertaken. Fig. 9 shows the magnetization versus the coercivity curves of $Fe_{65}Co_{35}$ prepared nanoparticles, at 300 K.

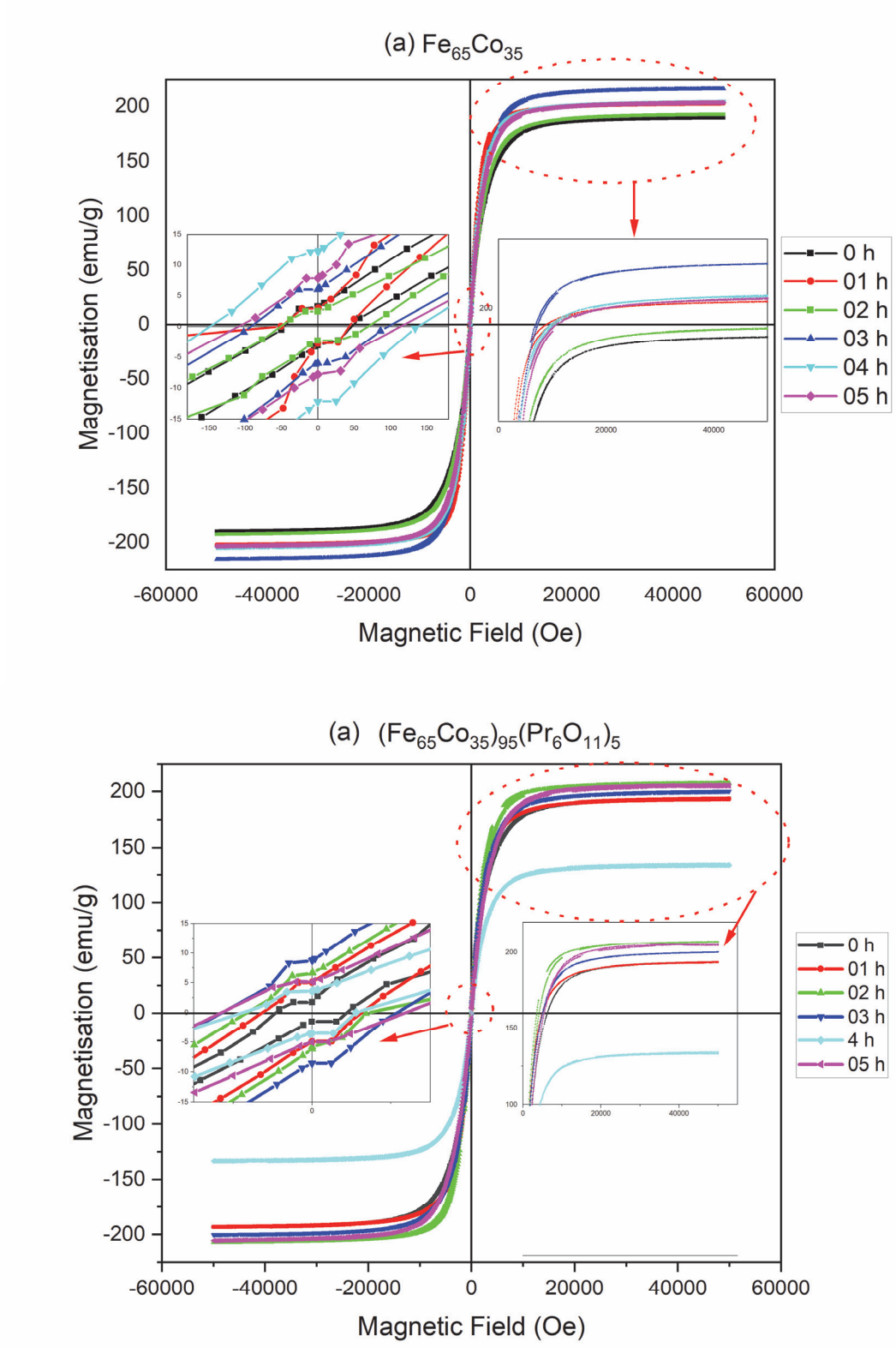

Figure 9: Hysteresis loops of $Fe_{65}Co_{35}$ and $(Fe_{65}Co_{35})_{95}(Pr_6O_{11})_5$ powders, at 300 K

Fig. 10 presents the magnetization saturation as a function of milling time curves of mechanically alloyed $Fe_{65}Co_{35}$ and $(Fe_{65}Co_{35})_{95}(Pr_6O_{11})_5$ powders, at 300 K.

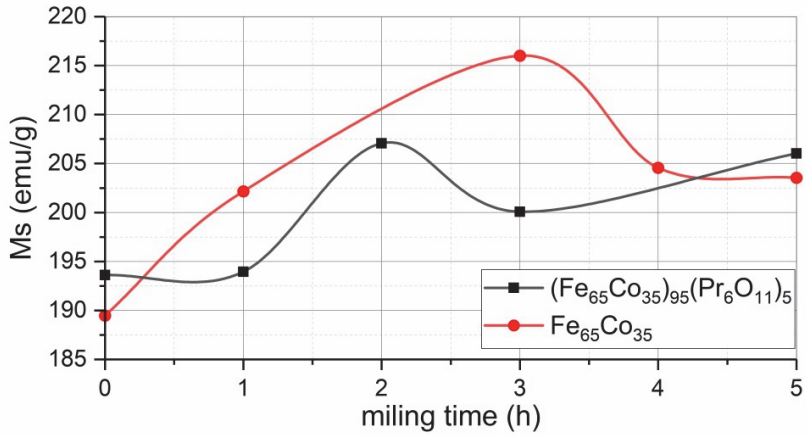

Figure 10: The saturation magnetization as a function of applied magnetic field curves of mechanically alloyed $Fe_{65}Co_{35}$ and $(Fe_{65}Co_{35})_{95}(Pr_6O_{11})_5$ powders, at 300 K

Firstly, for $Fe_{65}Co_{35}$, it is observed that M_s increases with milling time until reaching the maximum value of 216.01 emu/g after 3 h, before decreasing uniformly. This could be mainly attributed to the completion of the mechanisms allowing the formation of Fe-Co solid solution [57,62,63]. The decrement of M_s after 3 h of milling can be explained by the migration of Co atoms from Fe lattice to the grain boundaries [40,44]. For $(Fe_{65}Co_{35})_{95}(Pr_6O_{11})_5$ composition, M_s admits another behaviour: in the beginning, it increases to reach a maximum value of 207.06 emu/g after 2 h; after that, a decrease from 3 to 4 h is recorded and finally, M_s increases again until 5 h of milling. In order to explain this behaviour, it should be known that Fe and Co are ferromagnetic elements, whereas Pr is paramagnetic. As the evolution of M_s is mainly related to the local chemical composition of these elements inside the lattice, the initial increase of M_s can be explained by the fact that the dissolution of Co atoms inside the Fe lattice is dominant. Moreover, the decrease of M_s could be attributed to a significant change of the nearest neighbours configuration of ferromagnetic elements (Fe, Co) with the Pr paramagnetic. Another way to explain this fact is to take into account the modification of the 3d band structure responsible for ferromagnetism by the electrons brought by the praseodymium addition. The changes of the nearest neighbour configuration of Fe lead to the variation of the magnetic moment per atom and therefore the variation of the magnetization.

Fig. 11 presents the coercivity as a function of milling time curves of mechanically alloyed $Fe_{65}Co_{35}$ and $(Fe_{65}Co_{35})_{95}(Pr_6O_{11})_5$ powders, at 300 K.

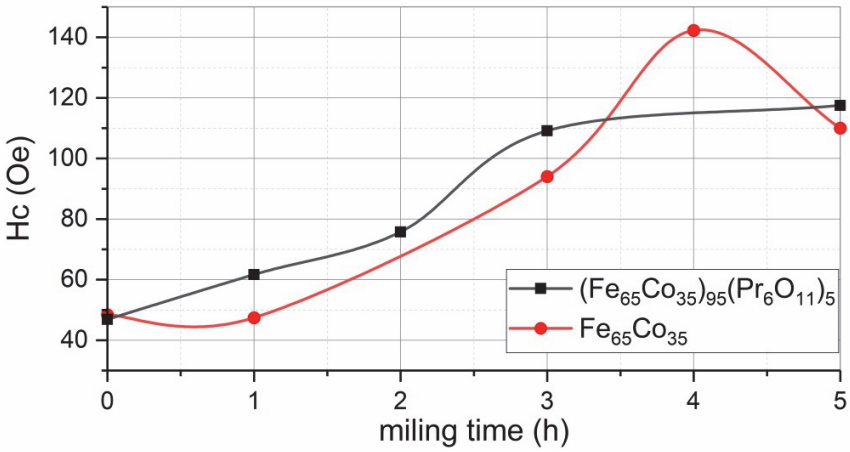

Figure 11: Coercivity as a function of applied magnetic field curves of mechanically alloyed $Fe_{65}Co_{35}$ and $(Fe_{65}Co_{35})_{95}(Pr_6O_{11})_5$ powders, at 300 K

It is clearly observed that the coercivity has a tendency to increase with milling time. An increment of H_c values from 47 Oe to 113 Oe in both compositions is detected. The increase of H_c is mainly due to the introduction of heavy plastic deformation during the MA process, which leads to the generation of defects and internal strain inside powders [2, 26]. The maximum achieved coercivity value is registered in $Fe_{65}Co_{35}$ samples milled for 4 h. Almost; this refers to the high

internal stress amount (~ 1 %) inside particles (Fig. 4). Moreover, the grain refinement has a significant effect on H_c values [64]. It is reported that for Fe-Co alloys, the critical particle diameter size corresponds to the multidomain-monodomain (MD-SD) transition is 50 nm [65], which is lower than the prepared particle size in this work (Fig. 6). Therefore, the coercivity dependence goes with 1/D. The decrement of H_c from 4 to 5 h in $Fe_{65}Co_{35}$ samples would be referred to the presence of small particles (< 50 nm) in which MD-SD transition occurs.
The structural stability was studied using the differential scanning calorimeter method.
Fig. 12 presents the DSC curves of $Fe_{65}Co_{35}$ and $(Fe_{65}Co_{35})_{95}(Pr_6O_{11})_5$ mechanically alloyed for 5 h.

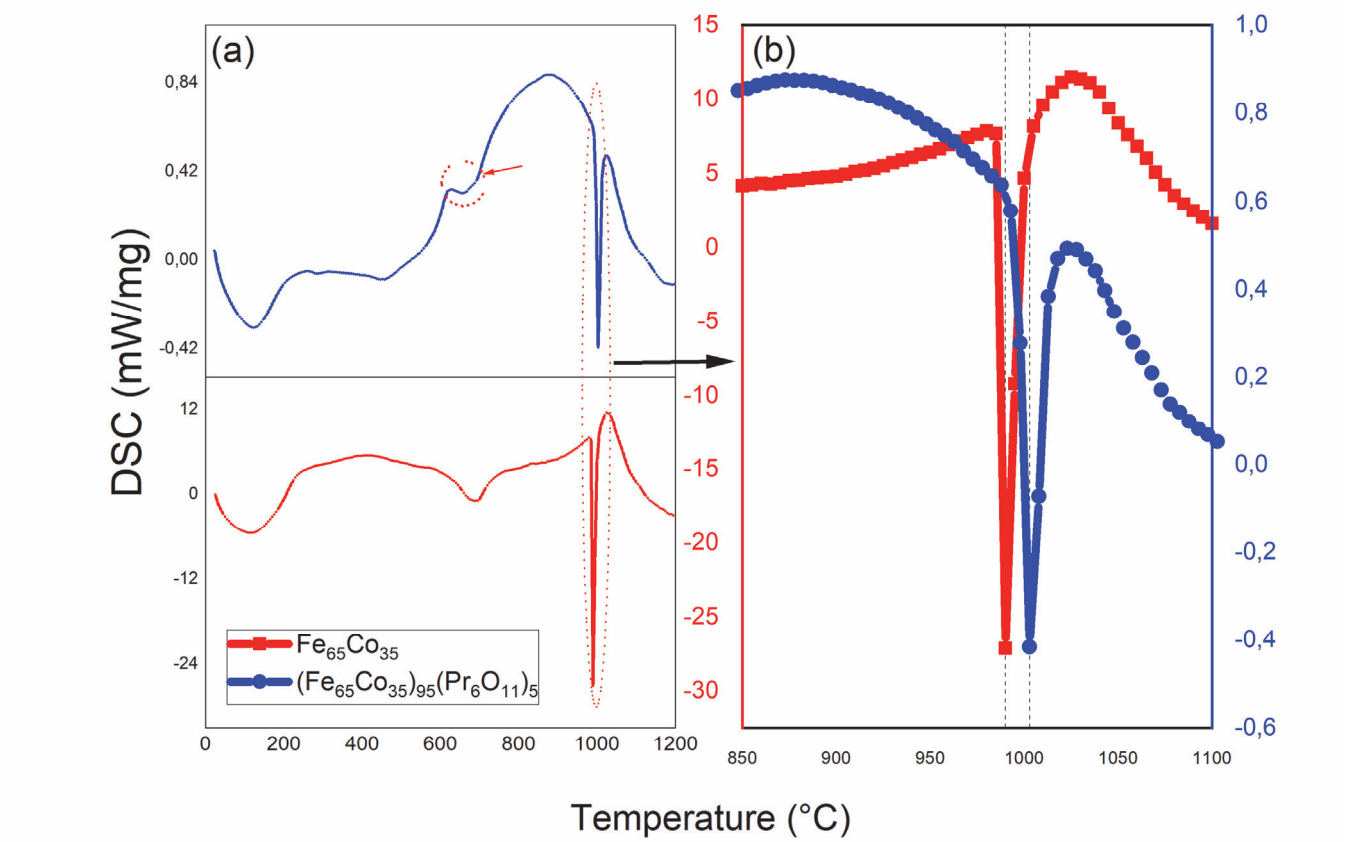

Figure 12: DSC scans of (a) $Fe_{65}Co_{35}$ and $(Fe_{65}Co_{35})_{95}(Pr_6O_{11})_5$ mechanically alloyed for 5 h and (b) zoom of the α–γ structural phase transition pic

The results confirm the formation of solid solutions. A broad exothermic peak occurs at the temperature range 110–120 °C in both alloys. This peak originates from recovery, strain relaxation, grain growth and recrystallization of nanocrystalline compositions [26]. The DSC scans for both alloys (Fig. 12.a) show the presence of two main exothermic peaks. The first one is broad with the onset temperature of 670-680 °C, which can be attributed to the disordered (bcc) – ordered B2 (bcc) structural transformation. This is in good accordance with the Fe–Co phase diagram [6,52]. the second sharp peak in both alloys is related to the transition from bcc ferromagnetic to the fcc paramagnetic structure [6]. Note that the onset temperature is 987 °C and 996.1 °C for $Fe_{65}Co_{35}$ and $(Fe_{65}Co_{35})_{95}(Pr_6O_{11})_5$ (Fig. 12-b). It seems that the Pr_6O_{11} addition stabilizes the bcc structure at high temperature and increases the magnetic order temperature of Fe-Co alloy.

Conclusions

In summary, nanocrystalline $(Fe_{65}Co_{35})_{100-x}$ $(Pr_6O_{11})_x$ (x = 0 and 5) alloys were successfully prepared by high energy ball milling. The microstructural investigation shows that 1 h of high energy milling is sufficient to dissolve Co and Pr_6O_{11} into the iron bcc structure. No additional phases were detected even the milling was carried out under air. The praseodymium oxide addition raises the decrement rate of crystallite size with milling time until 27 % because of its high

grain fragmentation tendency. Therefore, the internal microstrain in $(Fe_{65}Co_{35})_{95}(Pr_6O_{11})$ particles is 50 % lower than $Fe_{65}Co_{35}$ one. The lattice parameter decreased from 2.8660 nm for unmilled powders, to 2.860 and 2.862 nm for $Fe_{65}Co_{35}$and $(Fe_{65}Co_{35})_{95}(Pr_6O_{11})_5$ respectively. The decrement suggests that the Fe atoms are substituted by Co ones however Pr_6O_{11} does not dissolve into the $Fe_{65}Co_{35}$ crystal lattice but dispersed in the Fe–Co matrix, probably at the grain boundaries. The average particles size decreases in both compositions. Besides, $(Fe_{65}Co_{35})_{95}(Pr_6O_{11})_5$ powders are finer (1 μm) due to the fact that praseodymium oxide increases the hardness and brittleness of Fe-Co powders which minimize the cold welding between particles. Praseodymium addition slightly affects the high-magnetization ferromagnetic character of $Fe_{65}Co_{35}$ at 300 K. Furthermore, it does not affect the disordered (bcc) – ordered B2 (bcc) structural transformation of $Fe_{65}Co_{35}$. However, it stabilizes the bcc structure at high temperature and relatively increases the magnetic order temperature of $Fe_{65}Co_{35}$ alloy. The results obtained in this study reveal that high energy ball milling is a practical means for the synthesis of $(Fe_{65}Co_{35})_{95}(Pr_6O_{11})_5$ nanostructured powders as it provides excellent control over (1) crystallite size and residual microstrain, (2) particle size distribution, (3) structural integrity and homogenous dispersion of elements.

REFERENCES

[1] Garnero, C., Lepesant, M., Garcia-Marcelot, C., Shin, Y., Meny, C., Farger, P., Warot-Fonrose, B., Arenal, R., Viau, G., Soulantica, K., Fau, P., Poveda, P., Lacroix, L.M., Chaudret, B. (2019). Chemical Ordering in Bimetallic FeCo Nanoparticles: From a Direct Chemical Synthesis to Application As Efficient High-Frequency Magnetic Material, Nano Lett., 19(2), pp. 1379–1386, DOI: 10.1021/acs.nanolett.8b05083.

[2] Lu, G.D., Miao, X.S., Cheng, W.M., Huang, X.F., Yang, L., Pan, L.Q. (2015). Influence of Cu Underlayer on the High-Frequency Magnetic Properties of FeCoSiO Thin Films, IEEE Trans. Magn., 51(11), pp. 1–4, DOI: 10.1109/TMAG.2015.2438010.

[3] Khadra, G., Tamion, A., Tournus, F., Boisron, O., Albin, C., Dupuis, V. (2017). Structure and Magnetic Properties of FeCo Clusters: Carbon Environment and Annealing Effects, J. Phys. Chem. C, 121(20), pp. 10713–10718, DOI: 10.1021/acs.jpcc.6b10715.

[4] Shokrollahi, H., Janghorban, K. (2007). Soft magnetic composite materials (SMCs), J. Mater. Process. Technol., 189(1–3), pp. 1–12, DOI: 10.1016/j.jmatprotec.2007.02.034.

[5] Koohkan, R., Sharafi, S., Shokrollahi, H., Janghorban, K. (2008). Preparation of nanocrystalline Fe-Ni powders by mechanical alloying used in soft magnetic composites, J. Magn. Magn. Mater., 320(6), pp. 1089–1094, DOI: 10.1016/j.jmmm.2007.10.033.

[6] Sourmail, T. (2005). Near equiatomic FeCo alloys: Constitution, mechanical and magnetic properties, Prog. Mater. Sci., 50(7), pp. 816–880, DOI: 10.1016/j.pmatsci.2005.04.001.

[7] Delshad Chermahini, M., Sharafi, S., Shokrollahi, H., Zandrahimi, M., Shafyei, A. (2009). The evolution of heating rate on the microstructural and magnetic properties of milled nanostructured Fe1-xCox (x = 0.2, 0.3, 0.4, 0.5 and 0.7) powders, J. Alloys Compd., 484(1–2), pp. 54–58, DOI: 10.1016/j.jallcom.2009.05.055.

[8] Alonso, J., Khurshid, H., Sankar, V., Nemati, Z., Phan, M.H., Garayo, E., García, J.A., Srikanth, H. (2015). FeCo nanowires with enhanced heating powers and controllable dimensions for magnetic hyperthermia, J. Appl. Phys., 117(17), 17D113, DOI: 10.1063/1.4908300.

[9] Habib, A.H., Ondeck, C.L., Chaudhary, P., Bockstaller, M.R., McHenry, M.E. (2008). Evaluation of iron-cobalt/ferrite core-shell nanoparticles for cancer thermotherapy, J. Appl. Phys., 103(7), pp. 2012–2015, DOI: 10.1063/1.2830975.

[10] Hasegawa, T., Kanatani, S., Kazaana, M., Takahashi, K., Kumagai, K., Hirao, M., Ishio, S. (2017). Conversion of FeCo from soft to hard magnetic material by lattice engineering and nanopatterning, Sci. Rep., 7(1), pp. 1–7, DOI: 10.1038/s41598-017-13602-x.

[11] Seo, W.S., Lee, J.H., Sun, X., Suzuki, Y., Mann, D., Liu, Z., Terashima, M., Yang, P.C., McConnell, M. V., Nishimura, D.G., Dai, H. (2006). FeCo/graphitic-shell nanocrystals as advanced magnetic-resonance-imaging and near-infrared agents, Nat. Mater., 5(12), pp. 971–976, DOI: 10.1038/nmat1775.

[12] Zare, Y., Shams, M.H., Jazirehpour, M. (2017). Tuning microwave permittivity coefficients for enhancing electromagnetic wave absorption properties of FeCo alloy particles by means of sodium stearate surfactant, J. Alloys Compd., 717, pp. 294–302, DOI: 10.1016/j.jallcom.2017.05.043.

[13] Berasategi, J., Gomez, A., Bou-Ali, M.M., Gutiérrez, J., Barandiarán, J.M., Beketov, I. V., Safronov, A.P., Kurlyandskaya, G. V. (2018). Fe nanoparticles produced by electric explosion of wire for new generation of magneto-rheological fluids, Smart Mater. Struct., 27(4), 045011, DOI: 10.1088/1361-665X/aaaded.

[14] Bozorth, R.M. (1993). Ferromagnetism, New York, IEEE Press.
[15] Chen, C. (1977). Magnetism and Metallurgy of Soft Magnetic Materials, Holland Publishing Company.
[16] Klencsár, Z., Németh, P., Sándor, Z., Horváth, T., Sajó, I.E., Mészáros, S., Mantilla, J., Coaquira, J.A.H., Garg, V.K., Kuzmann, E., Tolnai, G. (2016). Structure and magnetism of Fe-Co alloy nanoparticles, J. Alloys Compd., 674, pp. 153–161, DOI: 10.1016/j.jallcom.2016.03.068.
[17] Krajewski, M., Tokarczyk, M., Stefaniuk, T., Lewinska, S., Slawska-Waniewska, A. (2019). Thermal Treatment of Chains of Amorphous Fe1-xCo Nanoparticles Made by Magnetic-Field-Induced Coreduction Reaction, IEEE Magn. Lett., 10, pp. 1–4, DOI: 10.1109/LMAG.2019.2950644.
[18] Yang, F.J., Yao, J., Min, J.J., Li, J.H., Chen, X.Q. (2016). Synthesis of high saturation magnetization FeCo nanoparticles by polyol reduction method, Chem. Phys. Lett., 648, pp. 143–146, DOI: 10.1016/j.cplett.2016.02.022.
[19] Yang, B., Wu, Y., Li, X., Yu, R. (2018). Chemical synthesis of high-stable amorphous feco nanoalloys with good magnetic properties, Nanomaterials, 8(3), 154, DOI: 10.3390/nano8030154.
[20] Lam, N.M., Thi, T.M., Thanh, P.T., Yen, N.H., Dan, N.H. (2018). Structure and magnetic properties of Fe-Co nanoparticles prepared by polyol method, Phys. B Condens. Matter, 532(November 2017), pp. 71–75, DOI: 10.1016/j.physb.2017.10.039.
[21] Vadillo, V., Gutierrez, J., Insausti, M., Garitaonandia, J.S., de Muro, I.G., Quintana, I., Barandiaran, J.M. (2019). Synthesis and characterization of Fe—Co—V high magnetization nanoparticles obtained by physical routes, IEEE Magn. Lett., 10, 6104805, DOI: 10.1109/LMAG.2019.2934076.
[22] Kanitz, A., Hoppius, J.S., del Mar Sanz, M., Maicas, M., Ostendorf, A., Gurevich, E.L. (2017). Synthesis of Magnetic Nanoparticles by Ultrashort Pulsed Laser Ablation of Iron in Different Liquids, ChemPhysChem, 18(9), pp. 1155–1164, DOI: 10.1002/cphc.201601252.
[23] Suryanarayana, C. (2008). Recent developments in mechanical alloying, Rev. Adv. Mater. Sci., 18(3), pp. 203–211, DOI: 10.1080/10667857.1994.11785013.
[24] Jing, Y., Sohn, H., Kline, T., Victora, R.H., Wang, J.P. (2009). Experimental and theoretical investigation of cubic FeCo nanoparticles for magnetic hyperthermia, J. Appl. Phys., 105(7), pp. 103–106, DOI: 10.1063/1.3074136.
[25] Azzaza, S., Alleg, S., Moumeni, H., Nemamcha, A.R., Rehspringer, J.L., Greneche, J.M. (2006). Magnetic properties of nanostructured ball-milled Fe and Fe 50Co50 alloy, J. Phys. Condens. Matter, 18(31), pp. 7257–7272, DOI: 10.1088/0953-8984/18/31/020.
[26] Poudyal, N., Rong, C., Zhang, Y., Wang, D., Kramer, M.J., Hebert, R.J., Ping Liu, J. (2012). Self-nanoscaling in FeCo alloys prepared via severe plastic deformation, J. Alloys Compd., 521, pp. 55–59, DOI: 10.1016/j.jallcom.2012.01.026.
[27] Razi, M., Ghasemi, A., Borhani, G.H. (2014). Microstructural and magnetic properties of nanostructured Fe65Co35 powders prepared by mechanical alloying, Adv. Mater. Res., 829(November 2013), pp. 778–783, DOI: 10.4028/www.scientific.net/AMR.829.778.
[28] Ge, S., Yao, D., Yamaguchi, M., Yang, X., Zuo, H., Ishii, T., Zhou, D., Li, F. (2007). Microstructure and magnetism of FeCo-SiO2 nano-granular films for high frequency application, J. Phys. D. Appl. Phys., 40(12), pp. 3660–3664, DOI: 10.1088/0022-3727/40/12/016.
[29] Enhanced magnetization in highly crystalline and atomically mixed bcc Fe-Co nanoalloys prepared by hydrogen reduction of oxide composites, Nanoscale, 5(4), pp. 1489–1493, DOI: 10.1039/c2nr33467d.
[30] Gupta, R., Gupta, A., Gupta, M., Rajput, P., Wildes, A. (2013). Evolution of structural and magnetic properties of amorphous CoFeB film with thermal annealing, J. Appl. Phys., 114(6), 063903, DOI: 10.1063/1.4817882.
[31] Hou, C., Shan, Y., Wu, H., Bi, X. (2013). Effect of a small addition of Cr on soft magnetic and mechanical properties of Fe-49Co-2V alloy, J. Alloys Compd., 556, pp. 51–55, DOI: 10.1016/j.jallcom.2012.12.044.
[32] Khosravi, S., Alizadeh, M., Sharafi, S., Karimi-Maleh, H., Atar, N. (2015). Structural, magnetic and electron transfer effect of Cr additive on Fe65Co35 nanopowder fabricated mechanical alloying, Powder Technol., 279, pp. 262–268, DOI: 10.1016/j.powtec.2015.04.019.
[33] Bouarroudj, T., Rida Benloucif, M., Mekki, D.E., Djekoun, M., Benamara, M., Berrebbeh, H. (2016). Cytotoxic effect of SnO2 nanoparticles on alternative cellular model: Paramecium tetraurelia, Stud. Univ. Vasile Goldis Arad, Ser. Stiint. Vietii, 26(3), pp. 323–30.
[34] K.SharmaR.V.Ramanujan, V.C.P. (2021). Accelerated study of magnetic Fe-Co-Ni alloys through compositionally graded spark plasma sintered samples, J. Alloys Compd., 869, pp. 159318.
[35] Jain, V., Chandra, A.R., Lakshmi, N., Reddy, V.R., Jani, S. (2019). Magnetic behaviour of 57 Fe/Co/Al multilayers deposited on a glass substrate, Bull. Mater. Sci., 42(4), pp. 1–6, DOI: 10.1007/s12034-019-1849-6.
[36] Sarkar, A., Hembram, S., Chatterjee, S., Basu Mallick, A. (2018). Effect of annealing treatments on the magnetic properties of FeCo/Cu core shell nanostructures, Mater. Today Proc., 5(1), pp. 745–751,

DOI: 10.1016/j.matpr.2017.11.142.
[37] Sarkar, A., Hembram, S., Chatterjee, S., Deb, P., Basu Mallick, A. (2017). Magnetic behaviour of FeCo/Cu core shell nanoparticles, Key Eng. Mater., 719(1), pp. 3–8, DOI: 10.4028/www.scientific.net/KEM.719.3.
[38] Xu, F., Xu, Z., Yin, Y. (2015). Tuning of the microwave magnetization dynamics in dy-doped Fe65Co35-Based Thin Films, IEEE Trans. Magn., 51(11), 2800904, DOI: 10.1109/TMAG.2015.2436053.
[39] Yousefi, M., Sharafi, S. (2012). The effect of simultaneous addition of Si and Co on microstructure and magnetic properties of nanostructured iron prepared by mechanical alloying, Mater. Des., 37, pp. 325–333, DOI: 10.1016/j.matdes.2012.01.011.
[40] Hocine, M., Guittoum, A., Hemmous, M., Martínez-Blanco, D., Gorria, P., Rahal, B., Blanco, J.A., Sunol, J.J., Laggoun, A. (2017). The role of silicon on the microstructure and magnetic behaviour of nanostructured (Fe0.7Co0.3)100−xSix powders, J. Magn. Magn. Mater., 422, pp. 149–156, DOI: 10.1016/j.jmmm.2016.08.058.
[41] Rincón Soler, A.I., Rodríguez Jacobo, R.R., Medina Barreto, M.H., Cruz-Muñoz, B. (2017). Structural and magnetic properties of FeCoC system obtained by mechanical alloying, Hyperfine Interact., 238(1), pp. 48–57, DOI: 10.1007/s10751-017-1419-5.
[42] Jung, I.H., Decterov, S.A., Pelton, A.D., Kim, H.M., Kang, Y.B. (2004). Thermodynamic evaluation and modeling of the Fe-Co-O system, Acta Mater., 52(2), pp. 507–519, DOI: 10.1016/j.actamat.2003.09.034.
[43] Shokrollahi, H. (2009). The magnetic and structural properties of the most important alloys of iron produced by mechanical alloying, Mater. Des., 30(9), pp. 3374–3387, DOI: 10.1016/j.matdes.2009.03.035.
[44] Farabi Khaneghahi, S., Sharafi, S. (2014). Magnetic and structural properties of nanostructured (Fe 65Co35)100-xCrx (x = 0, 10) powders prepared by mechanical alloying process, Adv. Powder Technol., 25(1), pp. 211–218, DOI: 10.1016/j.apt.2013.04.001.
[45] Chermahini, M.D., Sharafi, S., Shokrollahi, H., Zandrahimi, M. (2009). Microstructural and magnetic properties of nanostructured Fe and Fe50Co50 powders prepared by mechanical alloying, J. Alloys Compd., 474(1–2), pp. 18–22, DOI: 10.1016/j.jallcom.2008.06.144.
[46] Loudjani, N., Bensebaa, N., Dekhil, L., Alleg, S., Suñol, J.J. (2011). Structural and magnetic properties of Co50Ni50 powder mixtures, J. Magn. Magn. Mater., 323(23), pp. 3063–3070, DOI: 10.1016/j.jmmm.2011.06.059.
[47] Askeland, D.R.. (1994). The science and engineering of materials, Boston, PSW Publishing Company.
[48] Moumeni, H., Alleg, S., Greneche, J.M. (2005). Structural properties of Fe50Co50 nanostructured powder prepared by mechanical alloying, J. Alloys Compd., 386(1–2), pp. 12–19, DOI: 10.1016/j.jallcom.2004.05.017.
[49] Rathi, A., Meka, V.M., Jayaraman, T. V. (2019). Synthesis of nanocrystalline equiatomic nickel-cobalt-iron alloy powders by mechanical alloying and their structural and magnetic characterization, J. Magn. Magn. Mater., 469(September 2018), pp. 467–482, DOI: 10.1016/j.jmmm.2018.09.002.
[50] Cantor, B. (2005). Novel nanocrystalline alloys and magnetic nanomaterials, Oxford (UK), IOP.
[51] Fecht, H.J. (1995). Nanostructure formation by mechanical attrition, Nanostructured Mater., 6(1–4), pp. 33–42, DOI: 10.1016/0965-9773(95)00027-5.
[52] Chitsazan, B., Shokrollahi, H., Behvandi, A., Mirzaee, O. (2011). Characterization and magnetic coercivity of nanostructured (Fe 50Co 50) 100-XV X=0,2,4 powders containing a small amount of Co 3V intermetallic obtained by mechanical alloying, Powder Technol., 214(1), pp. 105–110, DOI: 10.1016/j.powtec.2011.07.042.
[53] Yousefi, M., Sharafi, S., Mehrolhosseiny, A. (2014). Correlation between structural parameters and magnetic properties of ball milled nano-crystalline Fe-Co-Si powders, Adv. Powder Technol., 25(2), pp. 752–760, DOI: 10.1016/j.apt.2013.11.008.
[54] Khajepour, M., Sharafi, S. (2011). Structural and magnetic properties of nanostructured Fe 50(Co50)-6.5 wt% Si powder prepared by high energy ball milling, J. Alloys Compd., 509(29), pp. 7729–7737, DOI: 10.1016/j.jallcom.2011.04.095.
[55] Gaffet, E. (1991). Planetary ball-milling: an experimental parameter phase diagram, Mater. Sci. Eng. A, 132(C), pp. 181–193, DOI: 10.1016/0921-5093(91)90374-V.
[56] Suryanarayana, C. (2001). Alliage mécanique et fraisage, Progrès En Sci. Des Matériaux, 46, pp. 1–184.
[57] Hosseini, H.R.M., Bahrami, A. (2005). Preparation of nanocrystalline Fe-Si-Ni soft magnetic powders by mechanical alloying, Mater. Sci. Eng. B Solid-State Mater. Adv. Technol., 123(1), pp. 74–79, DOI: 10.1016/j.mseb.2005.07.013.
[58] Chen, B., Li, S., Imai, H., Jia, L., Umeda, J., Takahashi, M., Kondoh, K. (2015). Load transfer strengthening in carbon nanotubes reinforced metal matrix composites via in-situ tensile tests, Compos. Sci. Technol., 113, pp. 1–8, DOI: 10.1016/j.compscitech.2015.03.009.
[59] Munir, K.S., Zheng, Y., Zhang, D., Lin, J., Li, Y., Wen, C. (2017). Microstructure and mechanical properties of carbon nanotubes reinforced titanium matrix composites fabricated via spark plasma sintering, Mater. Sci. Eng. A, 688, pp.

505–523, DOI: 10.1016/j.msea.2017.02.019.
[60] Zhang, H., Xu, C., Xiao, W., Ameyama, K., Ma, C. (2016). Enhanced mechanical properties of Al5083 alloy with graphene nanoplates prepared by ball milling and hot extrusion, Mater. Sci. Eng. A, 658, pp. 8–15, DOI: 10.1016/j.msea.2016.01.076.
[61] He, T., He, X., Tang, P., Chu, D., Wang, X., Li, P. (2017). The use of cryogenic milling to prepare high performance Al2009 matrix composites with dispersive carbon nanotubes, Mater. Des., 114, pp. 373–382, DOI: 10.1016/j.matdes.2016.11.008.
[62] Hamzaoui, R., Elkedim, O., Fenineche, N., Gaffet, E., Craven, J. (2003). Structure and magnetic properties of nanocrystalline mechanically alloyed Fe-10% Ni and Fe-20% Ni, Mater. Sci. Eng. A, 360(1–2), pp. 299–305, DOI: 10.1016/S0921-5093(03)00460-X.
[63] Hamzaoui, R., Elkedim, O., Gaffet, E., Greneche, J.M. (2006). Structure, magnetic and Mössbauer studies of mechanically alloyed Fe-20 wt.% Ni powders, J. Alloys Compd., 417(1–2), pp. 32–38, DOI: 10.1016/j.jallcom.2005.09.064.
[64] Zeng, Q., Baker, I., McCreary, V., Yan, Z. (2007). Soft ferromagnetism in nanostructured mechanical alloying FeCo-based powders, J. Magn. Magn. Mater., 318(1–2), pp. 28–38, DOI: 10.1016/j.jmmm.2007.04.037.
[65] Angelakeris, M. (2017). Magnetic nanoparticles: A multifunctional vehicle for modern theranostics, Biochim. Biophys. Acta - Gen. Subj., 1861(6), pp. 1642–1651, DOI: 10.1016/j.bbagen.2017.02.022.